Ultrasound in Med. & Biol., Vol. 45, No. 8, pp. 2049–2062, 2019

0301-5629/$ - see front matter

https://doi.org/10.1016/j.ultrasmedbio.2019.03.021

● *Original Contribution*

CHARACTERIZING FATTY LIVER *IN VIVO* IN RABBITS, USING QUANTITATIVE ULTRASOUND

Trong N. Nguyen, Anthony S. Podkowa, Alex Y. Tam, Eben C. Arnold, Rita J. Miller, Trevor H. Park, Minh N. Do, and Michael L. Oelze

Beckman Institute for Advanced Science and Technology, Department of Electrical and Computer Engineering, University of Illinois at Urbana-Champaign, Urbana, IL, USA

(*Received* 9 *October* 2018; *revised* 6 *March* 2019; *in final from* 28 *March* 2019)

Abstract—Nonalcoholic fatty liver disease (NAFLD) is the most common cause of chronic liver disease and can often lead to fibrosis, cirrhosis, cancer and complete liver failure. Liver biopsy is the current standard of care to quantify hepatic steatosis, but it comes with increased patient risk and only samples a small portion of the liver. Imaging approaches to assess NAFLD include proton density fat fraction estimated *via* magnetic resonance imaging (MRI) and shear wave elastography. However, MRI is expensive and shear wave elastography is not proven to be sensitive to fat content of the liver (Kramer et al. 2016). On the other hand, ultrasonic attenuation and the backscatter coefficient (BSC) have been observed to be sensitive to levels of fat in the liver (Lin et al. 2015; Paige et al. 2017). In this study, we assessed the use of attenuation and the BSC to quantify hepatic steatosis *in vivo* in a rabbit model of fatty liver. Rabbits were maintained on a high-fat diet for 0, 1, 2, 3 or 6 wk, with 3 rabbits per diet group (total $N = 15$). An array transducer (L9-4) with a center frequency of 4.5 MHz connected to a Sonix-One scanner was used to gather radio frequency (RF) backscattered data *in vivo* from rabbits. The RF signals were used to estimate an average attenuation and BSC for each rabbit. Two approaches were used to parameterize the BSC (*i.e.,* the effective scatterer diameter and effective acoustic concentration using a spherical Gaussian model and a model-free approach using a principal component analysis [PCA]). The 2 major components of the PCA from the BSCs, which captured 96% of the variance of the transformed data, were used to generate input features to a support vector machine for classification. Rabbits were separated into two liver fat-level classes, such that approximately half of the rabbits were in the low-lipid class (≤9% lipid liver level) and half of the rabbits in the high-lipid class (>9% lipid liver level). The slope and the midband fit of the attenuation coefficient provided statistically significant differences (p value = 0.00014 and p value = 0.007, using a two-sample t test) between low and high-lipid fat classes. The proposed model-free and model-based parameterization of the BSC and attenuation coefficient parameters yielded classification accuracies of 84.11 %, 82.93 % and 78.91 % for differentiating low-lipid versus high-lipid classes, respectively. The results suggest that attenuation and BSC analysis can differentiate low-fat versus high-fat livers in a rabbit model of fatty liver disease. (E-mail: oelze@illinois.edu)

Key Words: **Fatty liver, QUS, PCA, SVM.**

INTRODUCTION

Nonalcoholic fatty liver disease (NAFLD) is the most common chronic liver disease in humans and its prevalence continues to be on the rise (Wieckowska and Feldstein 2008). NAFLD is often used to describe the following range of liver conditions: fatty liver, steatohepatitis, advanced fibrosis and cirrhosis (Angulo 2002). Furthermore, patients with NAFLD may be at a greater risk of cardiovascular disease (Targher 2007). NAFLD affects both children and adults and is considered to be a serious health risk (Angulo 2002). With up to one-third of the US population affected by NAFLD (70%–90% of obese or type 2 diabetic patients have NAFLD), it represents a significant medical concern. In the spectrum of NAFLD, falling between steatosis and cirrhosis is nonalcoholic steatohepatitis (NASH). NASH has been estimated to be present in one-third of NAFLD cases (Farrell and Larter 2006). NASH is a serious condition that can progress to even more serious conditions such as cirrhosis, liver failure and hepatocarcinoma (Adams et al. 2005; Dam-Larsen et al. 2004; Ekstedt et al. 2006; Matteoni et al. 1999). The economic burden of this

Address correspondence to: Michael L Oelze, Beckman Institute, 405 N. Mathews, Urbana, IL, 61801 USA. E-mail: oelze@illinois.edu

disease has been estimated to be $103 billion in the United States and €35 billion in the United Kingdom, Germany, France and Italy combined (Younossi et al. 2016). Because NAFLD spans a range of medical conditions, from benign to serious, it is important to develop a sensitive and specific screening tool to classify and quantify NAFLD (Adams et al. 2005; Marchesini et al. 2005; McCullough 2004).

Currently, a liver biopsy continues to be the gold standard for the diagnosis of NAFLD. Histopathologic assessment of NASH includes detection of fatty changes to the hepatocytes with nuclear displacement to the edges of the cell and ballooning of the cells (Yeh and Brunt 2007). Other features, such as glycogenated nuclei and perisinusoidal/pericellular fibrosis, may be present but may not be required to establish a diagnosis of NASH (Brunt 2007; Wieckowska and Feldstein 2008). Attempts have been made to develop a standardized histologic diagnostic scoring system, called the NAFLD activity score (Kleiner et al. 2005; Sumida et al. 2011). The utility of this scoring system is still under investigation and is not meant to replace the diagnosis offered by a trained pathologist.

Even with a standardized metric for the diagnosis of NASH, several limitations are associated with a liver biopsy and its use as a screening tool (Sumida et al. 2014). One major limitation of a liver biopsy is the "sampling" problem. Liver biopsies sample as little as 1/50,000 of the total mass of the liver, which can result in insufficient data to make a proper diagnosis (Janiec et al. 2005; Merriman et al. 2006; Ratziu et al. 2005). Second, histologic analysis remains subjective and depends on the experience and abilities of the pathologist (Kleiner et al. 2005). Third, liver biopsy is an invasive procedure, which is stressful and financially costly to the patient. Finally, the invasiveness of the biopsy is not without potential significant complications, which can occur in ~0.5% of cases (Wieckowska and Feldstein 2008).

Laboratory tests for detecting and evaluating patients with suspected NAFLD include a serum panel of liver tests (Petäjä et al. 2016; Wieckowska and Feldstein 2008). However, these tests are far from perfect. For example, it has been demonstrated that normal values for certain liver tests (*e.g.,* levels of alanine aminotransferase) can span the full spectrum of NAFLD (Mofrad et al. 2003). Additional studies (enhanced liver fibrosis blood test and FibroTest) have demonstrated that many of these serum panels are not sensitive to both steatosis and fibrosis and cannot differentiate all stages of fibrosis (Baranova and Younossi 2008; Carey and Carey 2010; Friedrich-Rust et al. 2010; Guha et al. 2008; Lindor et al. 2004).

Various imaging techniques have been examined for improving the diagnosis of diffuse liver disease (Kramer et al. 2016; Mehta et al. 2008; Pacifico et al. 2007; Qayyum et al. 2009). For example, magnetic resonance imaging (MRI) with proton density fat fraction (PDFF) has been demonstrated to detect liver steatosis with higher sensitivity than conventional ultrasound (Cassidy et al. 2009; Mehta et al. 2008; Tang et al. 2015). However, MRI is expensive and the sensitivity and specificity of MRI for quantifying NAFLD and differentiating between fatty liver, NASH and fibrosis are insufficient (Kalra et al. 2009; Mehta et al. 2008). Because of the many people affected by fatty liver disease, MRI may be infeasible (Lin et al. 2015; Tang et al. 2015). Furthermore, in a study by Saadeh et al. (2002) on 90 patients with biopsy-proven NAFLD, it was observed that X-ray computed tomography (CT), ultrasound and MRI could not accurately distinguish between NASH and isolated fatty liver. Finally, X-ray CT utilizes ionizing radiation, which raises concerns regarding long-term safety.

Conventional ultrasound B-mode images have been used to detect NAFLD in cases of fatty liver because liver echogenicity increases with the severity of NAFLD, but with low sensitivity [Pamilo et al 1983; Celle et al. 1988]. Although conventional ultrasound can successfully diagnose some liver conditions, there are several weaknesses with the use of conventional ultrasound for detection of liver disease. First, current conventional ultrasonic techniques do not allow the quantification of the degree of fatty liver. Second, the effectiveness of ultrasound for liver disease detection is reduced in patients that are morbidly obese (sensitivity is reduced to below 40% [Almeida et al. 2008]). Third, for conventional ultrasound to detect steatosis, the degree of fat infiltration in the liver must be higher than 30% (Almeida et al. 2008; Dam-Larsen et al. 2004; Fishbein et al. 1997; Mehta et al. 2008). Fourth, conventional ultrasonic imaging is highly subjective and depends on the expertise and experience of the operator (Zwiebel 1995). Finally, conventional ultrasound has been unable to diagnose NASH and hepatic fibrosis or quantify the degree of fibrosis.

Other novel ultrasonic imaging techniques have been proposed and studied for their ability to overcome some of the deficiencies of conventional ultrasound, such as estimating the hepatorenal index, contrast imaging or transient elastography (TE) (Iijima et al. 2007; Kim et al. 2005; Ma et al. 2009). Among these techniques, recent attention has focused on TE methods for diagnosing diffuse liver disease. TE is a novel ultrasonic imaging technique that was initially validated in patients with chronic hepatitis C, with diagnostic performance similar to that of serum markers for diagnosis of significant fibrosis (Sandrin et al. 2003). The hypothesis behind TE is that fibrosis results in increased "stiffness" of the liver (Wells 2005). Some successes have been demonstrated for the ability to detect fibrosis,

especially when combined with serum panel tests (*i.e.,* FibroTest [Castera et al. 2005, 2008; Castera and Pawlotsky 2005; Ziol et al. 2005]). However, even with its ability to detect fibrosis, TE is insensitive to the fatty liver and cannot detect NAFLD. A more recent parameter, controlled attenuation parameter (CAP), is a supplementary feature during liver stiffness measurements (LSM) *via* vibration-controlled TE implemented by FibroScan (Echosens, Paris, France [Sasso, et al. 2010]) used for measuring the attenuation coefficient at 3.5 MHz. CAP has shown to be correlated to histologically determined steatosis (Karlas et al. 2017). However, CAP algorithms are proprietary, only displayed when LSM is valid and have limited applicability in obese patients (Petta et al. 2011).

Quantitative ultrasound (QUS) techniques based on attenuation estimation have also been examined for monitoring normal liver (Zagzebski et al. 1993) and a variety of disease conditions (Afschrift et al. 1987; Lizzi et al. 1988; Lu et al. 1997, 1999; Nicoll et al. 1998; O'Brien et al. 1996; Oosterveld et al. 1993; Suzuki et al. 1992; Thijssen et al. 1993). One of the earliest studies involved estimating attenuation in the liver to quantify diffuse liver disease (Suzuki et al. 1992). The slope of attenuation was estimated from ultrasound backscatter and correlated to pathologic findings (liver biopsy). Low values for attenuation slope were associated with chronic hepatitis. These early studies were followed by additional studies using attenuation to diagnose and grade liver disease (Suzuki et al. 1992). In a study using a rabbit model of fatty and fibrotic livers, attenuation was observed to depend on the fat content of the liver and to a lesser extent on the fibrotic content. In another set of studies, multiple QUS parameters were examined for liver disease diagnosis, including the following: attenuation, envelope statistics (1st order statistics) and power-spectral analysis (2nd order statistics [Oosterveld et al. 1993; Thijssen et al. 1993]). These studies used QUS parameters to detect the classes of diffuse liver disease against a population of normal livers. The researchers found that attenuation, envelope statistics, and spectral parameters were highly important parameters for discriminating various disease states. Similarly, Lizzi et al. (1988) examined scattering models and spectral analysis from backscattered ultrasound to interpret liver state. By providing parameters related to the tissue microstructure, they argued that better interpretation and insights into disease states could be obtained (Lizzi et al. 1988; Nicholas 1982).

More recently, QUS approaches have been utilized to quantify fatty liver disease in humans (Lin et al. 2015; Paige et al. 2017). In one study, the average backscatter coefficient (BSC) was estimated for patients and compared with MRI-PDFF estimates of fatty liver (Lin et al. 2015). The BSC was observed to correlate with the MRI-PDFF. Furthermore, using a cohort of 204 patients with NAFLD, the BSC was able to correctly identify patients with NAFLD with an area under the curve of 0.98. In a follow-up study, QUS was compared with conventional ultrasound and MRI-PDFF for predicting the grade of steatosis in 61 human patients (Paige et al. 2017). In that study, the BSC and attenuation were utilized for grading the degree of steatosis. The pilot study indicated that QUS was better at grading steatosis than conventional ultrasound but was not better than MRI-PDFF.

In our earlier study, excised livers from rabbits that were on a high-fat diet were assessed using QUS (Ghoshal et al. 2012). Both envelope statistics parameters using the homodyned K distribution and spectral-based parameters utilizing a spherical Gaussian form factor were used to help classify the liver into fatty versus non-fatty. Rabbits were labeled based on the number of weeks on the high-fat diet (0, 3 and 6 wk on the diet) and based on the Folch assay, which provided the percent lipid levels in the liver (Folch et al. 1957). The study found that the effective scatterer diameter (ESD) decreased from 31 to 17 μm, and the effective acoustic concentration (EAC) increased from 38 to 63 dB/cm^2 with the increase of weeks on the high-fat diet. Furthermore, envelope statistics parameters also tracked the degree of liver fat in the rabbit livers.

The earlier study was limited in that it utilized excised liver samples from the rabbits and relied on models of scattering to parameterize the liver state. In addition, ultrasonic interrogation occurred at frequencies higher than 8 MHz, which is high for abdominal imaging in humans. In this study, rabbits were on a high-fat diet for 0, 1, 2, 3 or 6 wk and livers were scanned in live rabbits, using ultrasonic frequencies lower than 8 MHz. QUS analysis was conducted using both a model-based approach (spherical Gaussian model) and a model-free approach (principal component analysis [PCA]) and compared. Under the Gaussian scattering model assumption, ESD and EAC can be estimated. This parametric approach assumes a scattering model that is usually unknown *a priori* and does not capture all of the nuances in the BSC. PCA is a data transformation and reduction method to extract new features from the BSC curves, which might be ignored through a spherical Gaussian form factor that is parameterized by simply fitting a line to the log-reduced BSC curve. A support vector machine (SVM) was utilized to quantify the classification accuracy instead of using descriptive statistics. The goal was to have the flexibility to tune the decision boundary of the classifier and visualize the boundary between classes. In addition, attenuation coefficients were

estimated *in vivo* and examined for their ability to differentiate liver state in live rabbits.

MATERIALS AND METHODS

Animal Procedures

The protocol was approved by the Institutional Animal Care and Use Committee at the University of Illinois at Urbana-Champaign. A total of 15 male New Zealand White rabbits were used in the study. Each group of rabbits was on a controlled diet for up to 6 wk. Specifically, they were transitioned from normal chow to a high-fat diet throughout a 10-d period during which the portion of the high-fat diet was increased 10% daily from 100% chow to 100% high-fat diet (King, et al. 2009). There were 5 different groups of rabbits with 3 rabbits per group and each group corresponding to a different number of weeks on the high-fat diet, *i.e.,* 0, 1, 2, 3 or 6 wk.

All rabbits were age matched and kept in house 11 wk before scanning. After the 11 wk, rabbits were returned to normal chow 1 wk before scanning with ultrasound. During scanning, the rabbits were anesthetized with isoflurane. The area over the liver was shaved and depilated before scanning. After scanning, the rabbits were euthanized while still under anesthesia. Immediately after euthanasia, the liver was removed *en mass.* A portion was flash frozen in liquid nitrogen and stored at −80 ˚C for use in the Folch assay.

Ultrasonic Scanning Procedures

The liver was scanned *in vivo* with an L9-4/38 transducer using the SonixOne system (Analogueic Corporation, Boston, MA, USA), providing an analysis bandwidth of 3−6 MHz. A total of 50 frames of post-beamformed radio frequency (RF) data sampled at 40 MHz were acquired for each rabbit and saved for off-line processing. A well-characterized reference phantom was scanned using the same system and system settings. The composition and acoustic properties of the reference phantom was presented in Nam et al. (2012). The reference phantom scan was used for calibration of the BSC and attenuation estimation (Yao et al. 1990).

Liver Fat Assessment

To correlate the ultrasonic-based parameters with the amount of fat content in the liver, the Folch assay was carried out on the rabbit livers after scanning (Folch 1957). Immediately after scanning and while still under anesthesia, the rabbits were euthanized, and the livers were extracted. Each liver was then weighed, and sections were excised, flash frozen in liquid nitrogen and stored in a −80 ˚C freezer. The Folch assay was conducted to determine the lipid percentage in the extracted livers. These values were used as the labels for the degree of fatty liver. The rabbits were divided into two classes based on the liver lipid percentage: class 0 included lipid percentage less than or equal to 9% and class 1 included lipid percentage greater than 9%. The 9% threshold was chosen because this resulted in approximately half of the rabbits below and half of the rabbits above the threshold (*i.e.,* 7 rabbits in class 0 and 8 rabbits in class 1).

QUS Processing

B-mode images of the livers were constructed from the raw RF data to manually segment out regions of data corresponding to the liver (*i.e.,* regions of interest were chosen for each frame). Care was taken to omit regions in the liver that were shadowed by the ribs or other structures or that contained large blood vessels. This region of interest was divided into various data blocks of size of 15 by 15 wavelengths (4.5 mm by 4.5 mm) of the center frequency of the array probe, (*i.e.,* 4.5 MHz). Each data block had a 75% overlap with other data blocks. The BSC was calculated for each data block, using the reference phantom method (Yao et al. 1990). Frequency-dependent attenuation was compensated in the BSC estimate through calculation of the local attenuation in the liver and then using the local attenuation value for the liver to calculate the total attenuation from the transducer surface to the region of interrogation. Because of the specular signals coming from the layers between the transducer and liver, it was not possible to estimate the local attenuation in these layers. This inability to properly account for the layer attenuation and loss is a source of error in the BSC estimates.

The BSC represents the normalized backscattered power per unit volume of scatterers and is a fundamental property of tissue like the attenuation. The BSC provides a curve of magnitude of the scattered power versus frequency over the analysis bandwidth of the source, which in this case was 3.0−6.0 MHz. To characterize tissue state based on the BSC, the BSC is often parameterized with features related to the magnitude and shape of the BSC curve. Usually, this is accomplished through the use of models for scattering. However, the curve shape can also be parameterized without the use of a specific model. In this study, the BSC was parameterized using (1) a common scattering model, (*i.e.,* the spherical Gaussian form factor model), and (2) without adopting a model for scattering but utilizing PCA.

Attenuation was also calculated from these data blocks, using the spectral difference method (Parker and Waag 1983; Yao et al. 1990). The attenuation curve in each data block was estimated using the spectral difference method and averaged over all image frames to get a mean attenuation curve for each rabbit liver. A slope and a midband fit at 4.5 MHz were estimated from the fitted

line to the average attenuation curve. A two-sample t test was used to compare different values of attenuation slopes and midband fits to the lipid liver level.

To parameterize the BSC, the ESD and EAC were estimated using a spherical Gaussian form factor model. The BSC is related to the spherical Gaussian form factor as follows:

$$\sigma_b(f) = \frac{\pi^4}{36c^4} f^4 D^6 \left(\overline{n}\gamma_0^2\right) e^{-0.827\pi^2 D^2 f^2/c^2}, \quad (1)$$

where f is the center frequency (MHz), c is the speed of sound, D is the ESD and $n\gamma_0^2$ is the EAC (Insana and Hall 1990). Using the method of Oelze and Zachary (2002), the ESD and EAC can be estimated from the estimated BSC through a least-squares optimization. This provides two classification features for the two classes of fatty liver.

PCA finds a linear compression mapping matrix W to transform the BSC curve $\boldsymbol{x}$ to a lower dimensional representation $\boldsymbol{y} = W\boldsymbol{x}$. The matrix W needs to satisfy the property that the recovering matrix U applied to y gives the minimal distance between the original and recovered vectors:

$$W,\ U = \underset{W \in R^{n,d},\ U \in R^{d,n}}{\operatorname{argmin}} \sum_{i=1}^{m} \left|\left| x_i - UWx_i \right|\right|_2^2, \quad (2)$$

where d is the dimension of x, n is the desired dimension of the compressed representation y and m is the number of examples. The matrix W is orthonormal and can be constructed by the d left singular vectors of the covariance data matrix $\frac{1}{m-1}X^TX$ (and U composed of right singular vectors) [Shalev-Shwartz and Ben-David 2014]). The eigenvector corresponding to the highest eigenvalue is called the first principal component along which the data have the highest variance. The next principal component vector is perpendicular to the first principal component and captures the second largest variance. The lower dimension n is chosen to capture as much variance in the data as possible. For our data, using only 2 principal components captures 96% of the variance in the BSCs. To parameterize using the PCA, the first 2 PCA components can be compressed. The compressed representation $y = Wx$ can be used as features for classification. The two features, PCA 1 and PCA 2, are the projections of the BSC x onto the first and second principal components w_1 and w_2: $y_1 = w_1x$, $y_2 = w_2x$ where w_1 and w_2 are the first 2 rows of W. The dimension of w_1 and w_2 are the same of that of the BSC x (*i.e.,* the number of FFT points used to calculate the power spectrum).

Classification

The training/test data sets were constructed of the features extracted from the BSC curves (PCA or ESD/EAC) and the attenuation curves (slopes and midband fit), and the corresponding classes (low/high fat) based on the fat percentage estimated from the Folch assay. Because the number of rabbits was small, leave-one-out cross-validation was used to evaluate the accuracy of classification: 14 rabbits were used for training and 1 rabbit was used for testing and this process repeated 15 times to get the average accuracy. The average accuracy was calculated for the training and testing phases and for the 3 feature extraction methods: model-based versus model-free using the BSC, and combined features from the BSC and attenuation curves.

During training, the labels (Folch assay results) and the features (either ESD, EAC or PCA-derived features) were trained using a supervised SVM classifier to generate the decision boundary between the two classes. Because the features of the two classes were overlapping and the number of examples was small, a linear SVM was used instead of a kernel SVM to not introduce artificial bias in classification. The decision boundary divides the feature spaces into disjoint regions corresponding to their classes. To quantify the accuracy of the classifier, the features in the testing set were projected to the decision space to get the predicted label for each BSC curve in each data block. The predicted labels were then compared with the true labels (from the Folch assay) to calculate the accuracies. The accuracy is defined as follows:

$$A = \frac{1}{N}\sum_{i=1}^{N} I(y_i \neq \hat{y}_i), \quad (3)$$

where I is the indicator function, y_i is the true output, $\hat{y}_i$ is the predicted output and N is the number of examples in the test set.

The features from the BSC and attenuation curves can be combined to improve the classification results. Because they are not the same units and same length scale (Table 1), a logistic regression, rather than an SVM, was used to impose a weighted classifying scheme. Logistic regression maximizes the likelihood

Table 1. Average ESD, EAC and attenuation slope, midband fit

	ESD	EAC	Attenuation slope	Attenuation at 4.5 MHz
Low lipid (5.74 ± 2.11 %)	167.05 ± 13.26 μm	21.13 ± 5.23 dB/cm^3	0.06 ± 0.15 dB/cm/MHz	3.42 ± 0.85 dB/cm
High lipid (14.02 ± 3.25 %)	118.93 ± 31.17 μm	31.82 ± 6.85 dB/cm^3	1.09 dB ± 0.2 dB/cm/MHz	5.48 ± 1.38 dB/cm
p value	0.002	0.005	0.00014	0.007

function:

$$L(\theta|x) = \prod_i \Pr(y_i|x_i;\theta), \tag{4}$$

where the probability of a feature vector x_i is of class $y_i = 1$ and $y_i = 0$ are:

$$\Pr(Y = 1|X;\theta) = \frac{1}{1+e^{-\theta^T X}}, \tag{5}$$

and

$$\Pr(Y = 0|X;\theta) = 1 - \Pr(Y = 1|X;\theta) = \frac{e^{-\theta^T X}}{1+e^{-\theta^T X}}, \tag{6}$$

where $\theta^T X = \theta_1 x_1 + \theta_2 x_2 + \theta_3 x_3 + \theta_4 x_4 + \theta_5$.

As an example, one feature vector $X = (x_1, x_2, x_3, x_4)$ is composed of the extracted ESD, EAC from the BSC curve, attenuation slope and the attenuation midband fit from the attenuation curve. The weight of each feature (θ_1, θ_2, θ_3, θ_4) can be interpreted as relating to the log of the ratio of the probability as follows:

$$\theta^T X = -ln\frac{P(Y = 0|X;\theta)}{P(Y = 1|X;\theta)}. \tag{7}$$

If the feature x_1 increases by one unit, the odds ratio $P(Y = \frac{0|X;\theta)}{P(Y} = 1|X;\theta)$ decreases by a factor of $\exp(\theta_1)$.

RESULTS

The results from the Folch assay are provided in the box plot in Figure 1. The general trend was that the longer the rabbit was on the high-fat diet, the higher the lipid level percentage. For example, the lowest lipid percentage occurred for rabbits that were not on the high-fat diet and the highest lipid level recorded occurred for a rabbit on the high-fat diet for a total of 6 wk. The histopathology result was well-correlated with the Folch assay results. We observed no lipidosis in the control group (3.27%, 3.29%, 4.10%). For the rabbit with highest Folch score (lipid level percent 20.66%), it was the only rabbit to receive a steatosis grade 5 with severe hepatic lipidosis. The remaining rabbits received a steatosis grade of 1 (subtle, minimal hepatic lipidosis), 2 (mild hepatic lipidosis), 3 (moderate hepatic lipidosis) or 4 (marked hepatic lipidosis) by the pathologist. Similar to what was observed from histopathology in our earlier study for rabbits on a high-fat diet, fat vacuoles accumulated in the hepatocytes of the livers with higher lipid content causing the cells to swell in size (Ghoshal, et al. 2012).

Figure 2a presents the average attenuation slopes and midband fits at a frequency of 4.5 MHz and their standard deviations for 14 rabbits where the low-lipid class is presented (*blue*) and the high-lipid class is presented (*orange*). The extracted data block of rabbit 1 was too small to reliably estimate the attenuation. Therefore, the attenuation estimated from rabbit 2, having a similar liver lipid percentage level, was used for attenuation compensation for the estimation of the BSC curves of rabbit 1. The higher the fat percentage, the higher the slope and midband fit. For example, Figures 2b and 2c plot the attenuation slope and midband fit as a function

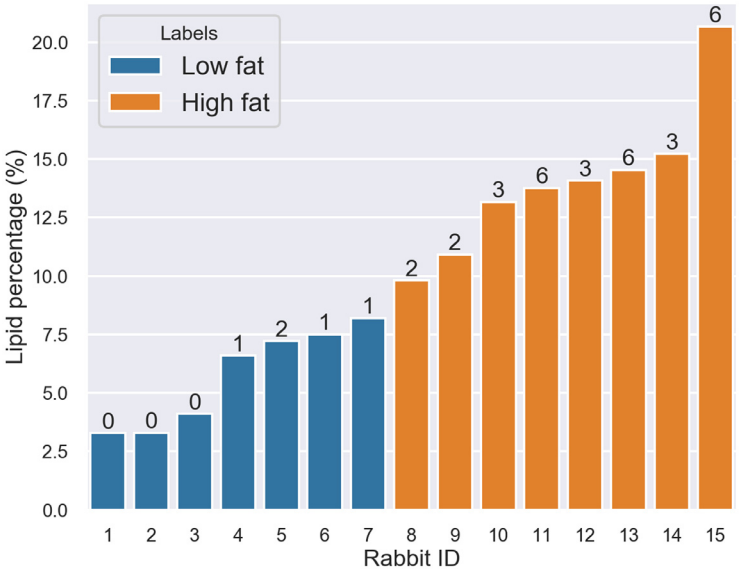

Fig. 1. Liver lipid percentages for 15 rabbits. Rabbits with lipid ≤9% are plotted in *blue*. Rabbits with lipid >9% are plotted in *orange*. The number of weeks on diet presented at top of each bar.

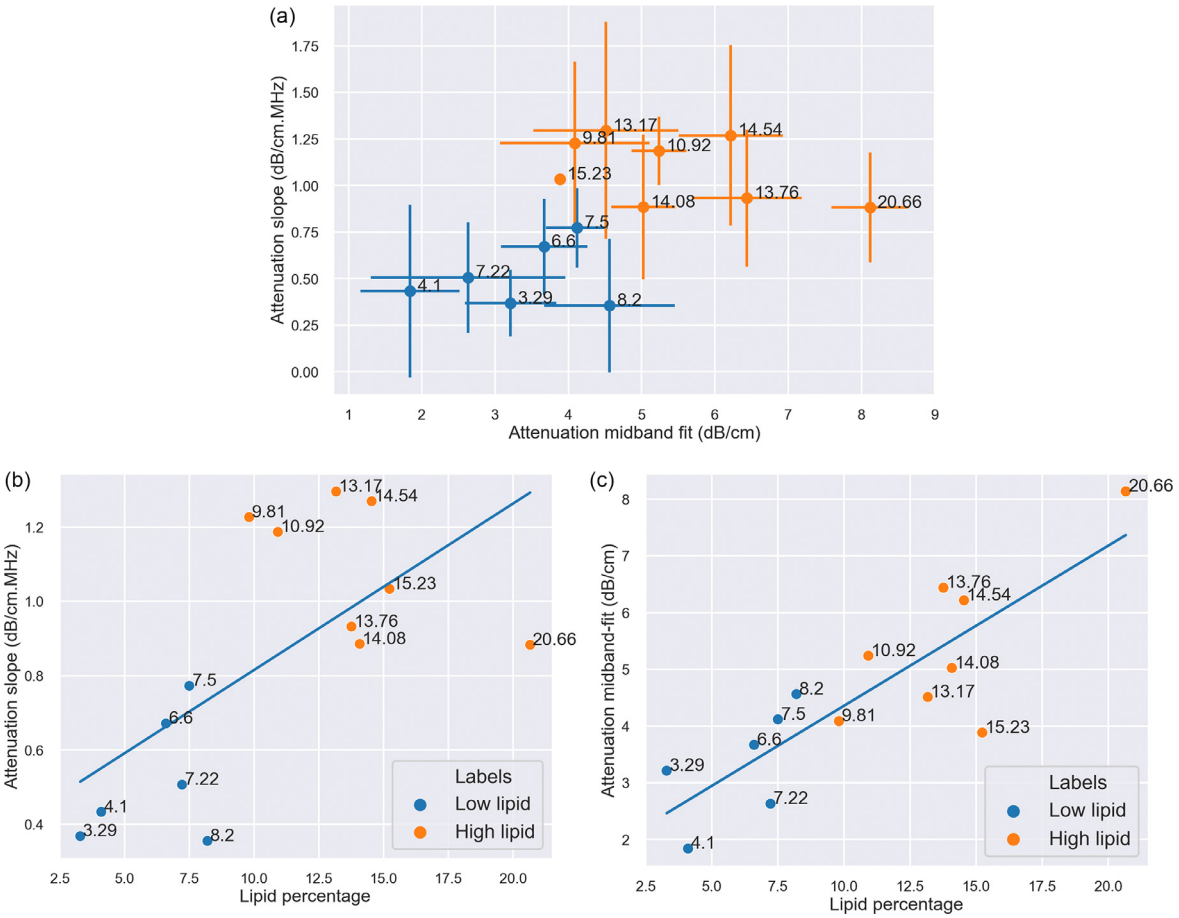

Fig. 2. (a) Attenuation slopes versus midband fits for 14 rabbits. Each circle point is the mean over all acquired frames. The bar represents the standard deviation. The lipid percentage is presented next to each data point. (b) The attenuation slopes versus lipid percentages for 14 rabbits. The straight line is the linear fit ($R^2 = 0.415$). (c) The attenuation midband fits versus lipid percentages for 14 rabbits. The straight line is the linear fit ($R^2 = 0.71$).

of the lipid percentage. Linear regression fits were also plotted with coefficients of determination of 0.415 and 0.71 for the attenuation slope and midband fit, respectively. The average slope and the average midband fit were extracted and are presented in Table 1 along with values estimated from the BSC (*i.e.,* ESD and EAC). Statistically significant differences were observed for the averaged slope and midband fit between the two classes. Another observation is that the rabbit with 20.66% had a similar attenuation slope as the rabbit with the Folch score of 7.5 %; however, the attenuation midband fit in dB/cm for the 20.66% rabbit was twice that of the 7.5% rabbit. Hence, the attenuation over the analysis bandwidth was still higher for the 20.66% rabbit than for the 7.5% rabbit.

Figure 3a presents the averaged BSC for all rabbits combined with low-lipid class and the high-lipid class. The graphs indicate that, as the fat in the liver increases, the BSC increases in magnitude, which has been demonstrated in other studies on fatty livers in rabbits (Ghoshal et al. 2012). The BSC was parameterized using a model-based and model-free approach to better classify the liver state. Figure 3b shows 2 examples of the averaged BSC and the standard deviations over 50 frames for 2 rabbits of ID 6 (lipid percentage 7.5 %) and ID 9 (lipid percentage 10.92 %).

Figure 4a plots the estimated averaged ESD and EAC and standard deviations computed from the BSCs, using the spherical Gaussian form factor and using attenuation compensation for each rabbit based on the attenuation estimates for that rabbit. Figures 4b and 4c plot the ESD and EAC as a function of the lipid percentage. Linear regression fits were also plotted with coefficients of determination of 0.23 and 0.47 for the ESD and EAC, respectively. The average ESD and EAC are summarized in Table 1 and plotted in Figure 5. Statistically significant differences between low-lipid and high-lipid classes were also observed using the ESD and EAC parameters ($p < 0.05$). Again, similar trends were noted in the *ex vivo* study of fatty rabbit livers where higher fat

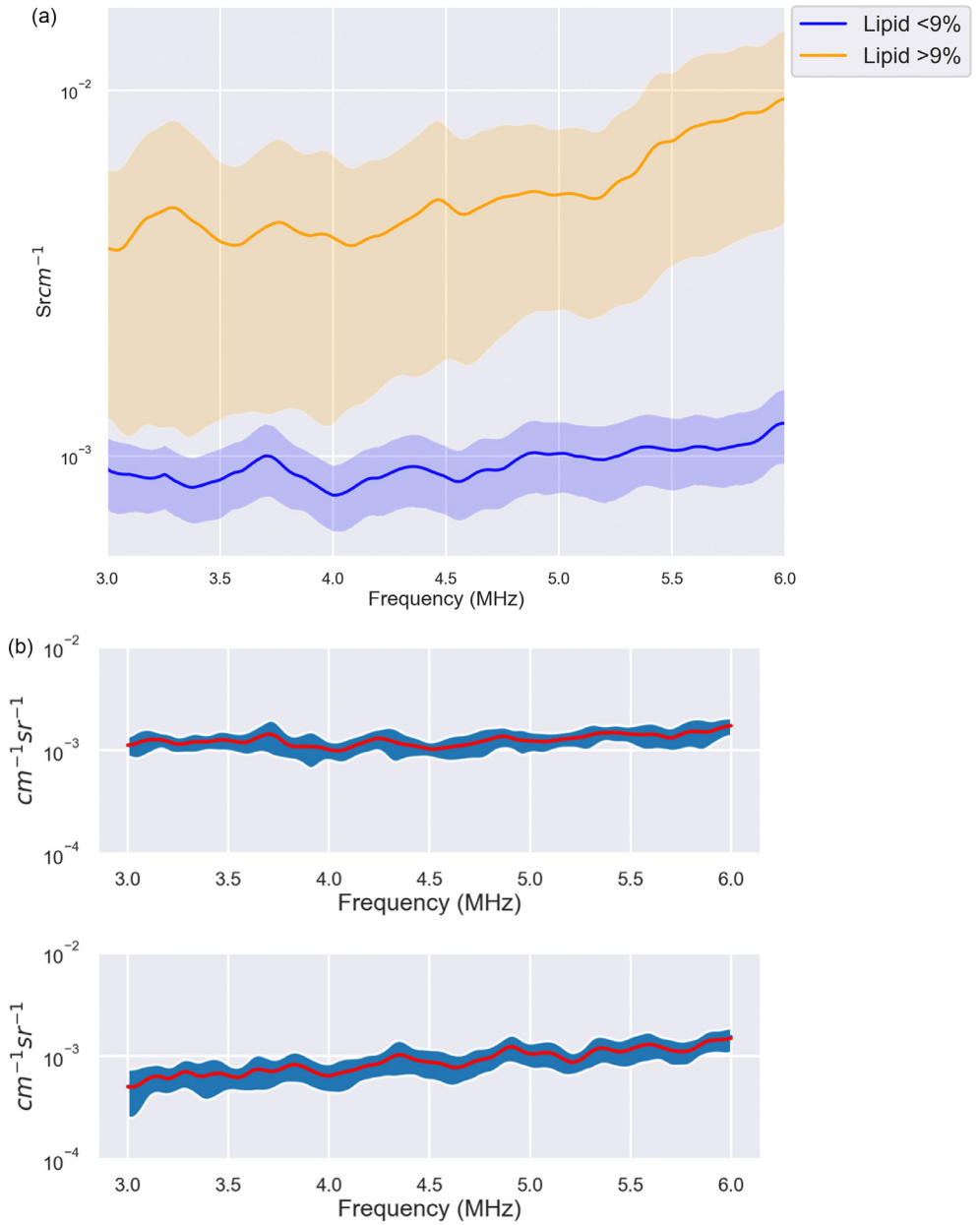

Fig. 3. (a) Average BSC of two classes: The higher lipid (>9%) BSC is presented in *orange*, the lower lipid (≤9%) is presented in *blue*. (b) The averaged BSCs (*red*) and standard deviations (*blue*) for 2 rabbits ID 6 (7.5 % lipid), and ID 9 (10.92 %) over 50 frames.

content resulted in estimates of smaller ESD but increases in EAC (Ghoshal et al. 2012).

Figure 5 presents plots of each individual parameter versus the lipid percentage level. The general trends indicate an increased attenuation slope, midband fit and EAC versus lipid level with some obvious outliers. Similarly, the ESD tended to decrease with higher lipid levels.

Table 2 lists the classification accuracies for the two classes with the 9% lipid-level threshold and using various ultrasound-based features. When comparing the BSC-based approaches, the PCA approach performed similarly to the model-based approach in both training and testing. Figure 6 shows a feature analysis of the 2 PCA collapsed components, indicating that the PCA was able to differentiate between the two classes of liver.

We implemented the classifier using two approaches: (1) classifying from every data block from each frame or (2) averaging the data blocks over a frame and classifying based on frames. Attenuation had a

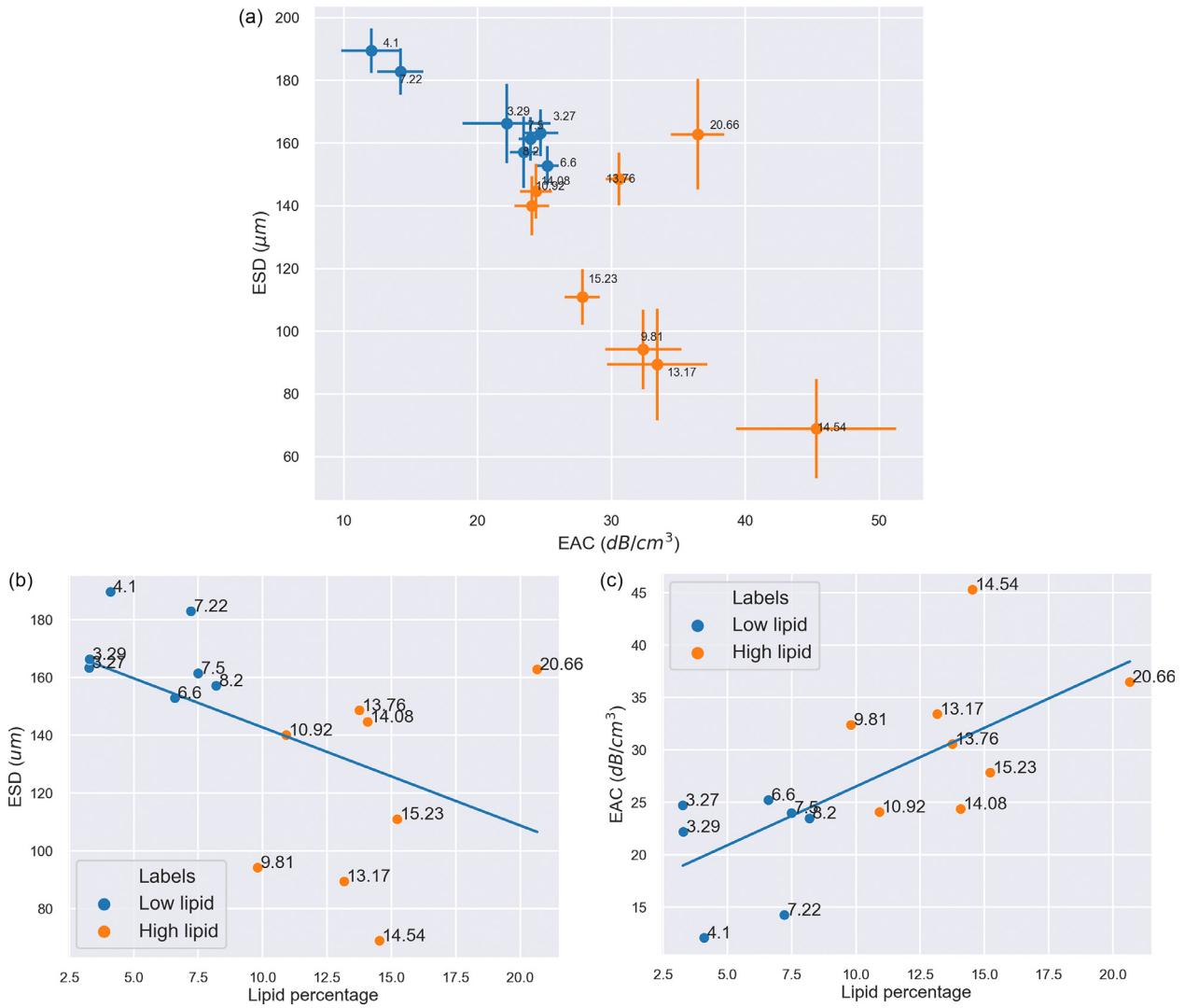

Fig. 4. (a) The averaged ESDs and EACs and their standard deviations of 15 rabbits. The lipid percentage is presented next to each data point. (b) ESDs versus lipid percentages for 14 rabbits. The straight line is the linear fit ($R^2 = 0.23$). (c) EACs versus lipid percentages for 14 rabbits. The straight line is the linear fit ($R^2 = 0.47$).

higher differentiation ability than the BSC when looking at the frame-based level and averaging over 50 frames (Table 2). However, the attenuation estimate variance for each frame was high, which reduced the accuracy of classification. The BSC estimates consistently had lower variances across data blocks and across frames and yielded similar classification results when using each data block and when averaging over a frame.

The features estimated from the BSC and the attenuation-based features were concatenated to classify by a logistic regression classifier. The results of the logistic regression classification using four concatenated features are provided in Table 2. The attenuation of rabbit 1 was not available and was not included in training and testing of the concatenated features. Combining ESD and EAC with attenuation slope and midband fit or the PCA features with the attenuation slope and midband fit improved the classification performance when using frame-based over the BSC-based features alone. The average weights for each feature when combining ESD, EAC with attenuation slope and midband fit across 15 testing folds are plotted in Figure 7. The ESD feature had negative weights, which agrees with the opposite changes observed with EAC in Table 1. ESD weights were the lowest in magnitude, to compensate for the large magnitudes of ESD features compared with the other features.

DISCUSSION

An *in vivo* rabbit model of fatty liver was used for testing the ability of QUS techniques to classify liver

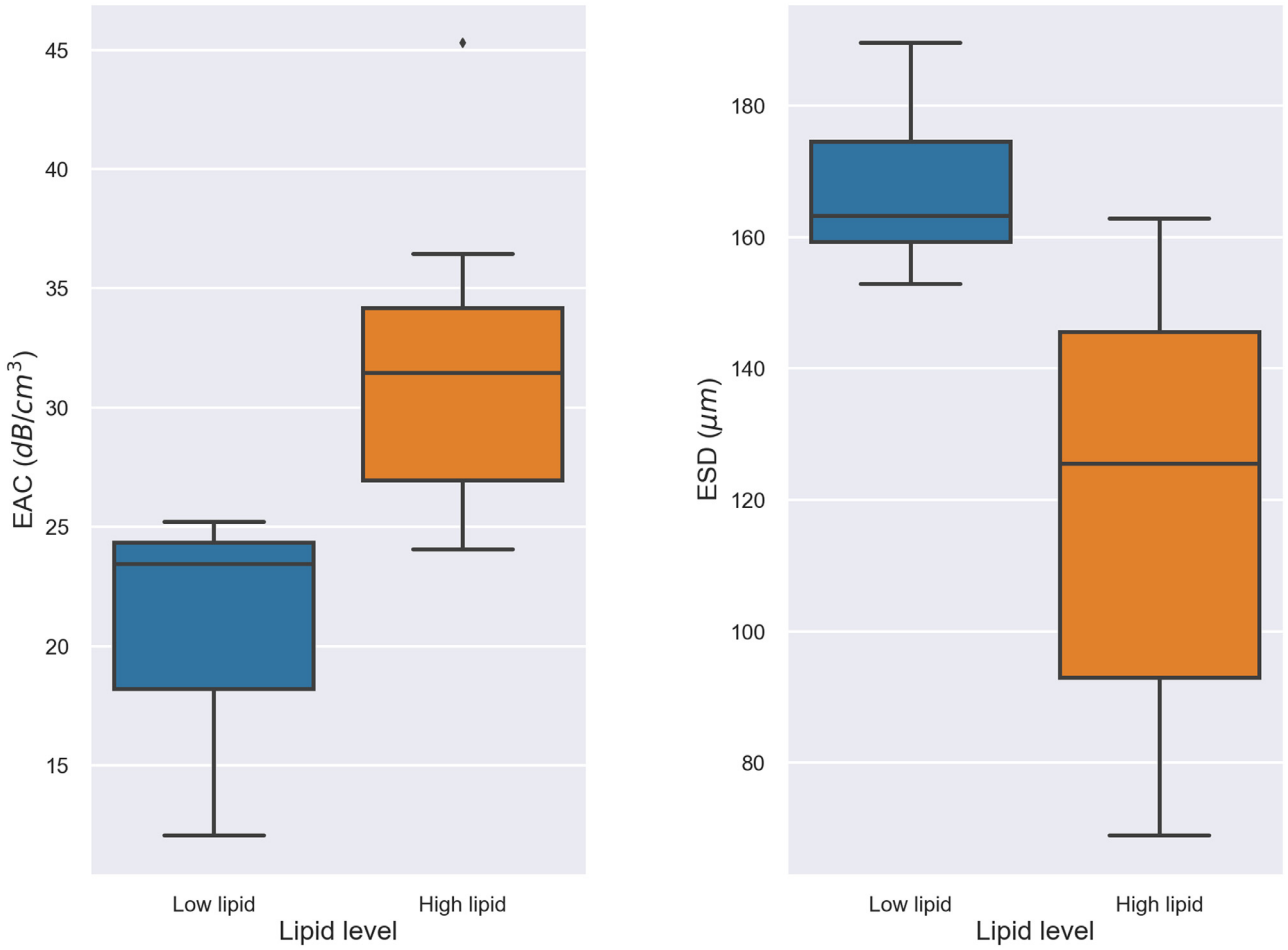

Fig. 5. Mean ESD and EAC for 2 lipid level classes. ESD, EAC features are statistically significant to differentiate the two classes (p value = 0.002, p value = 0.005).

Table 2. Blocked-based classification versus frame-based classification accuracy for various types of feature extraction methods

	Features	ESD and EAC	First 2 PCA components	Attenuation slope and midband fit	ESD, EAC, attenuation slope, attenuation midband fit	PCA 1, PCA 2, attenuation slope, attenuation midband fit
	Classifier	SVM (%)	SVM (%)	SVM (%)	Logistic regression (%)	Logistic regression (%)
Blocked based	Training accuracy	88.00	87.62	80.71	92.15	91.94
	Test accuracy	84.08	83.97	66.20	86.74	85.32
Frame based	Training accuracy	88.42	88.14	83.78	94.66	93.15
	Test accuracy	84.11	82.93	78.91	93.38	88.67

state into low-lipid and high-lipid classes. Rabbits were maintained on a high-fat diet for different numbers of weeks and then scanned ultrasonically. Specifically, QUS parameters from estimates of the attenuation and BSC were used to classify livers into a low and high liver lipid percentage. The total liver lipid percentages were estimated from the Folch assay and corresponded closely to the number of weeks on diet. The 9% threshold of liver lipid levels was chosen to obtain approximately the same number of rabbits into the two classes. A different threshold could be chosen based on clinical relevance. However, it should be noted that changing the threshold would also change the accuracy of the results presented in this study. For example, if the threshold was to change to 10%, the rabbit with the lipid of 9.81% would be misclassified, given its high-attenuation slope and low ESD.

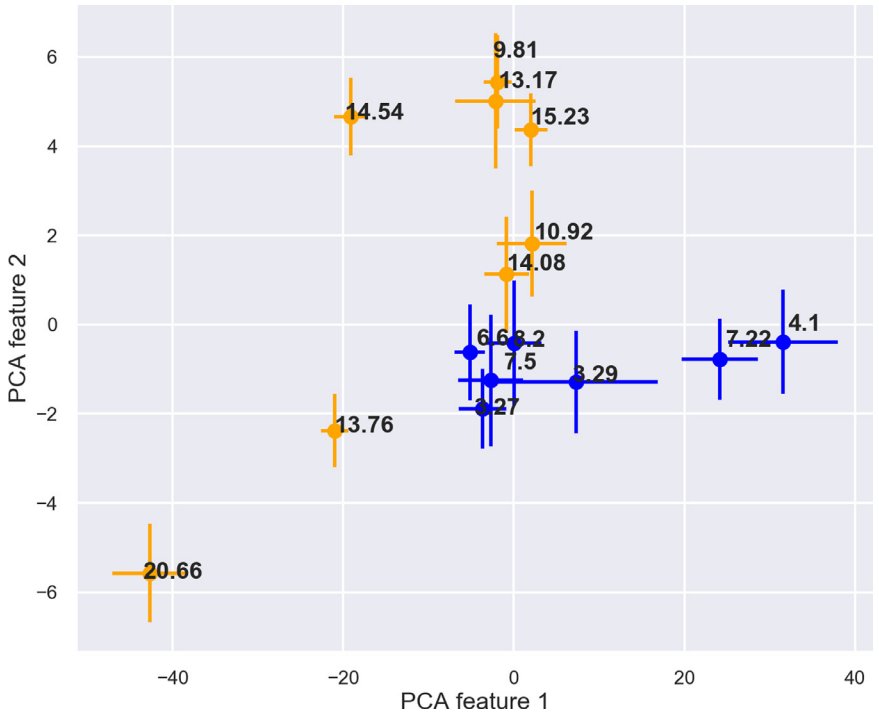

Fig. 6. Presented are 2 PCA features for 15 rabbits. The lipid percentage is presented next to each data point.

The p values are still strong for attenuation (p value = 0.006 for attenuation slope, p value = 0.002 for attenuation midband fit) and EAC (p = 0.025) but would be weaker for ESD (p value = 0.1) because of the very low ESD values obtained for this rabbit.

The R^2 values of individual QUS parameters and the lipid percentages were small, because there were high variances in QUS estimates, making them less linear. Even so, each individual parameter provided some predictive value for lipid liver percent, although in some cases the predictive capability of the individual features was low. However, when combining all QUS parameters in a linear model, the R^2 value was 0.79. An R^2 value of 0.79 signifies a strong predictive value of the combined feature set.

The attenuation and BSC demonstrated the ability to differentiate between low-lipid and high-lipid classes in live rabbits. Statistically significant differences (p value = 0.00014, and p value = 0.007 using the two-sample t test) were observed between the slope and the midband fit of the attenuation curves for the low-lipid and high-lipid level classes. The BSC-derived features using PCA performed similarly as the ESD and EAC features derived from a spherical Gaussian model for classifying the rabbits into low-fat and high-fat classes.

PCA features are more spatially compact than ESD and EAC features and potentially more robust to the noisy outliers. A simple monotonic change in the features versus increases in lipid levels were not observed. However, general trends were observed for the attenuation (*e.g.,* the slope tended to increase with increasing lipid levels). Other dimensionality reduction methods similar to PCA to find a compressed representation of the data exist such as local linear embedding (Roweis and Saul 2000) or multidimensional scaling (Kruskal 1964). However, PCA is generally more robust to noise in the data compared with the aforementioned methods.

The results from Table 2 suggest that to obtain good classification, the attenuation should be averaged over all the data blocks in an image frame to reduce the variance of the estimate. The variance in the BSC estimate is much lower per data block compared with the attenuation estimate. Majority voting over block prediction in each frame can be used to provide an average parameter estimate for an image frame. However, the improvement was insignificant and was not shown here.

In an attempt to improve the results of classification above that achieved using only the BSC-derived features or only the attenuation-derived features, the BSC-derived features were combined with attenuation curve features and the logistic regression classifier was used on the combined feature set. Logistic regression automatically scales the features, as shown in Figure 7. Improved classification with the combined set was observed over both, using BSC-derived features and using attenuation-derived features.

Variance in average parameter estimates from one rabbit to the next could account for some of the misclassification based on the feature sets. The variance of estimates from *in vivo* scanning was expected to be higher

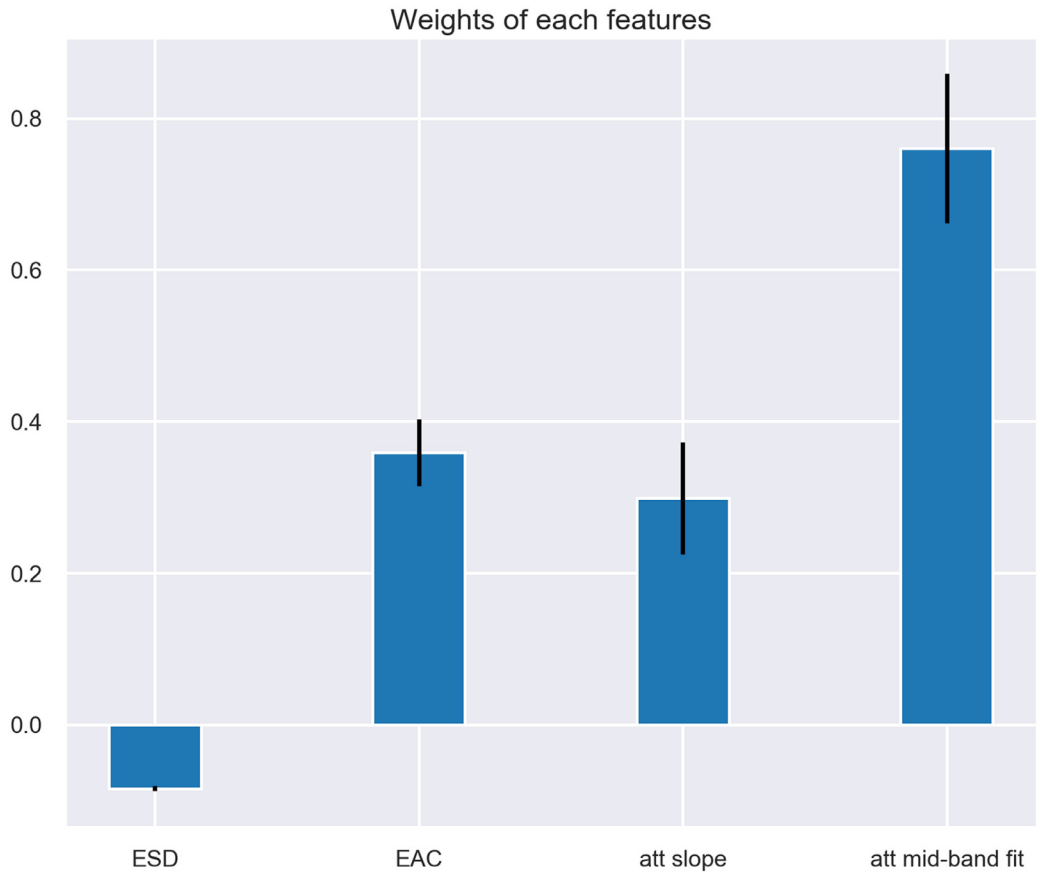

Fig. 7. The averaged weights across 14 validation folds of the 4 features of the trained logistic regression classifier. The ESD weights are negative and small compared with the others.

compared with an earlier study where excised liver samples from rabbits on a fatty diet were scanned (Ghoshal et al. 2012). In the *in vivo* data, intervening layers between the liver and the transducer were observed and these layers would affect the signal-to-noise ratio in the data, could result in contamination of the data from reverberation and provide frequency-dependent losses of signal not accounted for properly. A transmission loss estimation method might improve the accuracy of the classification by reducing the variance of estimates. In humans, this is expected to be more of a problem because layers between an ultrasonic probe and the liver can vary greatly in thickness and fat content resulting in a wider range of loss.

The lower accuracy of the classifier based on parameters derived from the attenuation compared with BSC curves are attributable to the variance of attenuation estimates within a single rabbit being higher than BSC estimates within a single rabbit. The misclassification of the BSC curves might be attributable to the transmission losses, inconsistent coupling from one rabbit to the next, unaccounted skin layer thickness of the rabbits and errors in the manual segmentation of the liver. Not accounting for these variations from one rabbit to the next would produce a higher variance of the average BSC estimates, which would degrade classification performance. As an example, although the Folch assay results provided similar values for rabbits with the 9.81% and 8.2%, their ESD and attenuation slope values differ by a factor of approximately 2 and 4, respectively. Correctly estimating the transmission loss or the attenuation in the layers between the transducer probe and the liver is still an open problem. However, it should be noted that estimation of attenuation from the backscatter is less likely to be impacted by these losses because the attenuation estimation technique uses relative estimates of power spectra from multiple depths. The effects of the layers on one depth should theoretically be the same at a slightly larger depth.

CONCLUSION

This study compared a model-based approach with a model-free approach to parameterize the BSC and classify livers from rabbits into low-lipid or high-lipid liver level classes. The model-free approach utilized the PCA to parameterize the BSC and classified using a

supervised SVM. Local attenuation estimation also provided the ability to classify rabbits into low-lipid and high-lipid liver classes. The BSC was not as strong for classifying the liver lipid levels into the two classes compared with attenuation alone. Combining BSC-based estimates with attenuation resulted in improved classification compared with the BSC-based estimates alone.

Acknowledgments—This work was supported by a grant from National Institutes of Health (NIH) (R21 EB020766). We wish to acknowledge the assistance of Prof. Matthew Wallig and his pathology expertise in this work.

REFERENCES

Adams LA, Lymp JF, St Sauver J, Sanderson SO, Lindor KD, Feldstein A, Angulo P. The natural history of nonalcoholic fatty liver disease: A population-based cohort study. Gastroenterology 2005;129:113–121.

Afschrift M, Cuvelier C, Ringoir S, Barbier F. Influence of pathological state on the acoustic attenuation coefficient slope of liver. Ultrasound Med Biol 1987;13:135–139.

Angulo P. Nonalcoholic fatty liver disease. N Engl J Med 2002; 346:1221–1231.

Baranova A, Younossi ZM. The future is around the corner: Noninvasive diagnosis of progressive nonalcoholic steatohepatitis. Hepatology 2008;47:373–375.

Brunt EM. Pathology of fatty liver disease. Mod Pathol 2007;20(Suppl 1): S40–S48.

Carey E, Carey WD. Noninvasive tests for liver disease, fibrosis, and cirrhosis: Is liver biopsy obsolete? Cleve Clin J Med 2010;77:519–527.

Cassidy FH, Yokoo T, Aganovic L, Hanna RF, Bydder M, Middleton MS, Hamilton G, Chavez AD, Schwimmer JB, Sirlin CB. Fatty liver disease: MR imaging techniques for the detection and quantification of liver steatosis. Radiographics 2009;29:231–260.

Castera L, Forns X, Alberti A. Non-invasive evaluation of liver fibrosis using transient elastography. J Hepatol 2008;48:835–847.

Castera L, Pawlotsky J-M. Noninvasive diagnosis of liver fibrosis in patients with chronic hepatitis C. MedGenMed 2005;7:39.

Castéra L, Vergniol J, Foucher J, Bail B, Chanteloup E, Haaser M, Darriet M, Couzigou P, de Lédinghen V. Prospective comparison of transient elastography, Fibrotest, APRI, and liver biopsy for the assessment of fibrosis in chronic hepatitis C. Gastroenterology 2005;128:343–350.

Celle G, Savarino V, Picciotto A, Magnolia MR, Scalabrini P, Dodero M. Is hepatic ultrasonography a valid alternative tool to liver biopsy? report on 507 cases studied with both techniques. Dig Dis Sci 1988;33:467–471.

Dam-Larsen S, Franzmann M, Andersen IB, Christoffersen P, Jensen LB, Sørensen TIA, Becker U, Bendtsen F. Long term prognosis of fatty liver: Risk of chronic liver disease and death. Gut 2004;53:750–755.

de Moura Almeida A, Cotrim HP, Barbosa DB, de Athayde LG, Santos AS, Bitencourt AG, de Freitas LA, Rios A, Alves E. Fatty liver disease in severe obese patients: Diagnostic value of abdominal ultrasound. World J Gastroenterol 2008;14:1415–1418.

Ekstedt M, Franzen LE, Mathiesen UL, Thorelius L, Holmqvist M, Bodemar G, Kechagias S. Long-term follow-up of patients with NAFLD and elevated liver enzymes. Hepatology 2006;44:865–873.

Farrell GC, Larter CZ. Nonalcoholic fatty liver disease: From steatosis to cirrhosis. Hepatology 2006;43(2 Suppl 1):S99–S112.

Fishbein MH, Gardner KG, Potter CJ, Schmalbrock P, Smith MA. Introduction of fast MR imaging in the assessment of hepatic steatosis. Magn Reson Imaging 1997;15:287–293.

Folch J, Lees M, Stanley SG. A simple method for the isolation and purification of total lipides from animal tissues. J Biol Chem 1957;226:497–509.

Friedrich-Rust M, Rosenberg W, Parkes J, Herrmann E, Zeuzem S, Sarrazin C. Comparison of ELF, FibroTest and FibroScan for the non-invasive assessment of liver fibrosis. BMC Gastroenterol 2010;10:103.

Ghoshal G, Lavarello RJ, Kemmerer JP, Miller RJ, Oelze ML. *Ex vivo* study of quantitative ultrasound parameters in fatty rabbit livers. Ultrasound Med Biol 2012;38:2238–2248.

Guha IN, Parkes J, Roderick P, Chattopadhyay D, Cross R, Harris S, Kaye P, Burt AD, Ryder SD, Aithal GP, Day CP, Rosenberg WM. Noninvasive markers of fibrosis in nonalcoholic fatty liver disease: Validating the European Liver Fibrosis Panel and exploring simple markers. Hepatology 2008;47:455–460.

Iijima H, Moriyasu F, Tsuchiya K, Suzuki S, Yoshida M, Shimizu M, Sasaki S, Nishiguchi S, Maeyama S. Decrease in accumulation of ultrasound contrast microbubbles in non-alcoholic steatohepatitis. Hepatol Res 2007;37:722–730.

Insana MF, Hall TJ. Parametric ultrasound imaging from backscatter coefficient measurements: Image formation and interpretation. Ultrason Imaging 1990;12:245–267.

Janiec DJ, Jacobson ER, Freeth A, Spaulding L, Blaszyk H. Histologic variation of grade and stage of non-alcoholic fatty liver disease in liver biopsies. Obes Surg 2005;15:497–501.

Kalra N, Duseja A, Das A, Dhiman R, Virmani V, Chawla Y, Singh P, Khandelwal N. Chemical shift magnetic resonance imaging is helpful in detecting hepatic steatosis but not fibrosis in patients with nonalcoholic fatty liver disease (NAFLD). Ann Hepatol 2009;8:21–25.

Karlas T, Petroff D, Sasso M, Fan JG, Mi YQ, de Ledinghen V, Kumar M, Lupsor-Platon M, Han KH, Cardoso AC, Ferraioli G, Chan WK, Wong VW, Myers RP, Chayama K, Friedrich-Rust M, Beaugrand M, Shen F, Hiriart JB, Sarin SK, Badea R, Jung KS, Marcellin P, Filice C, Mahadeva S, Wong GL, Crotty P, Masaki K, Bojunga J, Bedossa P, Keim V, Wiegand J. Individual patient data meta-analysis of controlled attenuation parameter (CAP) technology for assessing steatosis. J Hepatol 2017;66:1022–1030.

Kim S, Lee J, Lee J, Han J, An S, Han C, Lee K, Hwang S, Choi B. Value of contrast-enhanced sonography for the characterization of focal hepatic lesions in patients with diffuse liver disease: Receiver operating characteristic analysis. AJR Am J Roentgenol 2005;184:1077–1084.

King JL, Miller RJ, Blue JP, Jr., O'Brien WD, Jr., Erdman JW, Jr. Inadequate dietary magnesium intake increases atherosclerotic plaque development in rabbits. Nutr Res 2009;29:343–349.

Kleiner DE, Brunt EM, Van Natta M, Behling C, Contos MJ, Cummings OW, Ferrell LD, Liu YC, Torbenson MS, Unalp-Arida A, Yeh M, McCullough AJ, Sanyal AJ. Nonalcoholic Steatohepatitis Clinical Research Network. Design and validation of a histological scoring system for nonalcoholic fatty liver disease. Hepatology 2005;41:1313–1321.

Kramer H, Pickhardt PJ, Kliewer MA, Hernando D, Chen G-H, Zagzebski JA, Reeder SB. Accuracy of liver fat quantification with advanced CT, MRI, and ultrasound techniques: Prospective comparison with MR spectroscopy. AJR Am J Roentgenol 2016;208:92–100.

Kruskal JB. Multidimensional scaling by optimizing goodness of fit to a nonmetric hypothesis. Psychometrika 1964;29:1–27.

Lin SC, Heba E, Wolfson T, Ang B, Gamst A, Han A, Erdman JW, Jr., O'Brien WD, Jr., Andre MP, Sirlin CB, Loomba R. Noninvasive diagnosis of nonalcoholic fatty liver disease and quantification of liver fat using a new quantitative ultrasound technique. Clin Gastroenterol Hepatol 2015;13 1337−1345.e6.

Lindor KD, Kowdley KV, Heathcote EJ, Harrison ME, Jorgensen R, Angulo P, Lymp JF, Burgart L, Colin P. Ursodeoxycholic acid for treatment of nonalcoholic steatohepatitis: Results of a randomized trial. Hepatology 2004;39:770–778.

Lizzi FL, King DL, Rorke MC, Hui J, Ostromogilsky M, Yaremko MM, Feleppa EJ, Wai P. Comparison of theoretical scattering results and ultrasonic data from clinical liver examinations. Ultrasound Med Biol 1988;14:377–385.

Lu Z, Zagzebski JA, Lee FT. Ultrasound backscatter and attenuation in human liver with diffuse disease. Ultrasound Med Biol 1999;25:1047–1054.

Lu ZF, Zagzebski JA, O'Brien RT, Steinberg H. Ultrasound attenuation and backscatter in the liver during prednisone administration. Ultrasound Med Biol 1997;23:1–8.

Ma X, Holalkere N-S, Avinash KR, Mino-Kenudson M, Hahn PF, Sahani DV. Imaging-based quantification of hepatic fat: Methods and clinical applications. Radiographics 2009;1253–1277.

Marchesini G, Marzocchi R, Agostini F, Bugianesi E. Nonalcoholic fatty liver disease and the metabolic syndrome. Curr Opin Lipidol 2005;16:421–427.
Matteoni CA, Younossi ZM, Gramlich T, Boparai N, Liu YC, McCullough AJ. Nonalcoholic fatty liver disease: A spectrum of clinical and pathological severity. Gastroenterology 1999;116:1413–1419.
McCullough AJ. The clinical features, diagnosis and natural history of nonalcoholic fatty liver disease. Clin Liver Dis 2004;8:521–533.
Mehta SR, Thomas EL, Bell JD, Johnston DG, Taylor-Robinson SD. Non-invasive means of measuring hepatic fat content. World J Gastroenterol 2008;14:3476–3483.
Merriman RB, Ferrell LD, Patti MG, Weston SR, Pabst MS, Aouizerat BE, Bass NM. Correlation of paired liver biopsies in morbidly obese patients with suspected nonalcoholic fatty liver disease. Hepatology 2006;44:874–880.
Mofrad P, Contos MJ, Haque M, Sargeant C, Fisher RA, Luketic VA, Sterling RK, Shiffman ML, Stravitz RT, Sanyal AJ. Clinical and histologic spectrum of nonalcoholic fatty liver disease associated with normal ALT values. Hepatology 2003;37:1286–1292.
Nam K, Rosado-Mendez IM, Wirtzfeld LA, Kumar V, Madsen EL, Ghoshal G, Pawlicki AD, Oelze ML, Lavarello RJ, Bigelow TA, Zagzebski JA, O'Brien WD, Jr., Hall TJ. Cross-imaging system comparison of backscatter coefficient estimates from a tissue-mimicking material. J Acoust Soc Am 2012;132:1319–1324.
Nicholas D. Evaluation of backscattering coefficients for excised human tissues: Results, interpretation and associated measurements. Ultrasound Med Biol 1982;8:17–28.
Nicoll RG, Jackson MW, Knipp BS, Zagzebski JA, Steinberg H, O'Brien RT. Quantitative ultrasonography of the liver in cats during obesity induction and dietary restriction. Res Vet Sci 1998;64:1–6.
O'Brien RT, Zagzebski JA, Lu ZF, Steinberg H. Measurement of acoustic backscatter and attenuation in the liver of dogs with experimentally induced steroid hepatopathy. Am J Vet Res 1996;57:1690–1694.
Oelze ML, Zachary JF. Characterization of tissue microstructure using ultrasonic backscatter: Theory and technique for optimization using a Gaussian form factor. J Acoust Soc Am 2002;112:1202–1211.
Oosterveld BJ, Thijssen JM, Hartman PC, Rosenbusch GJ. Detection of diffuse liver disease by quantitative echography: Dependence on a priori choice of parameters. Ultrasound Med Biol 1993;19:21–25.
Pamilo M, Sotaniemi E, Suramo I, Lähde S , Arranto A. Evaluation of liver steatotic and fibrous content by computerized tomography and ultrasound. Scand J Gastroenterol 1983;18:743–747.
Pacifico L, Celestre M, Anania C, Paolantonio P, Chiesa C, Laghi A. MRI and ultrasound for hepatic fat quantification: Relationships to clinical and metabolic characteristics of pediatric nonalcoholic fatty liver disease. Acta Pediatr 2007;96:542–547.
Paige JS, Bernstein GS, Heba E, Costa EAC, Fereirra M, Wolfson T, Gamst AC, Valasek MA, Lin GY, Han A, Erdman JW, O'Brien WD, Andre MP, Loomba R, Sirlin CB. A pilot comparative study of quantitative ultrasound, conventional ultrasound, and MRI for predicting histology-determined steatosis grade in adult nonalcoholic fatty liver disease. AJR. Am J Roentgenol 2017;208:W168–W177.
Parker KJ, Waag RC. Measurement of ultrasonic-attenuation within regions selected from B-scan images. IEEE Trans Biomed Eng 1983;30:431–437.
Petäjä EM, Zhou Y, Havana M, Hakkarainen A, Lundbom N, Ihalainen J, Yki-Järvinen H. Phosphorylated IGFBP-1 as a non-invasive predictor of liver fat in NAFLD. Sci Rep 2016;6:24740.
Petta S, Di Marco V, Camma C, Butera G, Cabibi D, Craxi A. Reliability of liver stiffness measurement in non-alcoholic fatty liver disease: The effects of body mass index. Aliment Pharmacol Ther 2011;33:1350–1360.
Qayyum A, Chen DM, Breiman RS, Westphalen AC, Yeh BM, Jones KD, Lu Y, Coakley FV, Callen PW. Evaluation of diffuse liver steatosis by ultrasound, computed tomography, and magnetic resonance imaging: Which modality is best? Clin Imaging 2009;33:110–115.
Ratziu V, Charlotte F, Heurtier A, Gombert S, Giral P, Bruckert E, Grimaldi A, Capron F, Poynard T. LIDO Study Group. Sampling variability of liver biopsy in nonalcoholic fatty liver disease. Gastroenterology 2005;128:1898–1906.
Roweis ST, Saul LK. Nonlinear dimensionality reduction by locally linear embedding. Science 2000;290:2323–2326.
Saadeh S, Younossi ZM, Remer EM, Gramlich T, Ong JP, Hurley M, Mullen KD, Cooper JN, Sheridan MJ. The utility of radiological imaging in nonalcoholic fatty liver disease. Gastroenterology 2002;123:745–750.
Sandrin L, Fourquet B, Hasquenoph J-M, Yon S, Fournier C, Mal F, Christidis C, Ziol M, Poulet B, Kazemi F, Beaugrand M, Palau R. Transient elastography: A new noninvasive method for assessment of hepatic fibrosis. Ultrasound Med Biol 2003;29:1705–1713.
Sasso M, Beaugrand M, de Ledinghen V, Douvin C, Marcellin P, Poupon R, Sandrin L, Miette V. Controlled attenuation parameter (CAP): A novel VCTE^{TM} guided ultrasonic attenuation measurement for the evaluation of hepatic steatosis: Preliminary study and validation in a cohort of patients with chronic liver disease from various causes. Ultrasound Med Biol 2010;36:1825–1835.
Shalev-Shwartz S, Ben-David S. Understanding machine learning: From theory to algorithms. Cambridge: Cambridge University Press; 2014.
Sumida Y, Nakajima A, Itoh Y. Limitations of liver biopsy and noninvasive diagnostic tests for the diagnosis of nonalcoholic fatty liver disease/nonalcoholic steatohepatitis. World J Gastroenterol 2014;20:475–485.
Sumida Y, Yoneda M, Hyogo H, Yamaguchi K, Ono M, Fujii H, Eguchi Y, Suzuki Y, Imai S, Kanemasa K, Fujita K, Chayama K, Yasui K, Saibara T, Kawada N, Fujimoto K, Kohgo Y, Okanoue T. Jsg-Nafld. A simple clinical scoring system using ferritin, fasting insulin, and type IV collagen 7 S for predicting steatohepatitis in nonalcoholic fatty liver disease. J Gastroenterol 2011;46:257–268.
Suzuki K, Hayashi N, Sasaki Y, Kono M, Kasahara A, Fusamoto H, Imai Y, Kamada T. Dependence of ultrasonic attenuation of liver on pathologic fat and fibrosis: Examination with experimental fatty liver and liver fibrosis models. Ultrasound Med Biol 1992;18:657–666.
Tang A, Desai A, Hamilton G, Wolfson T, Gamst A, Lam J, Clark L, Hooker J, Chavez T, Ang BD, Middleton MS, Peterson M, Loomba R, Sirlin CB. Accuracy of MR imaging-estimated proton density fat fraction for classification of dichotomized histologic steatosis grades in nonalcoholic fatty liver disease. Radiology 2015;274:416–425.
Targher G. Non-alcoholic fatty liver disease, the metabolic syndrome and the risk of cardiovascular disease: The plot thickens. Diabet Med 2007;24:1–6.
Thijssen JM, Oosterveld BJ, Hartman PC, Rosenbusch GJE. Correlations between acoustic and texture parameters from RF and B-mode liver echograms. Ultrasound Med Biol 1993;19:13–20.
Wells RG. The role of matrix stiffness in hepatic stellate cell activation and liver fibrosis. J Clin Gastroenterol 2005;39(4 Suppl 2):S158–S161.
Wieckowska A, Feldstein AE. Diagnosis of nonalcoholic fatty liver disease: Invasive versus noninvasive. Semin Liver Dis 2008;28:386–395.
Yao LX, Zagzebski JA, Madsen EL. Backscatter coefficient measurements using a reference phantom to extract depth-dependent instrumentation factors. Ultrason Imaging 1990;12:58–70.
Yeh MM, Brunt EM. Pathology of nonalcoholic fatty liver disease. Am J Clin Pathol 2007;128:837–847.
Younossi ZM, Blissett D, Blissett R, Henry L, Stepanova M, Younossi Y, Racila A, Hunt S, Beckerman R. The economic and clinical burden of nonalcoholic fatty liver disease in the United States and Europe. Hepatology 2016;64:1577–1586.
Zagzebski JA, Lu ZF, Yao LX. Quantitative ultrasound imaging: *In vivo* results in normal liver. Ultrason Imaging 1993;15:335–351.
Ziol M, Handra-Luca A, Kettaneh A, Christidis C, Mal F, Kazemi F, de Lédinghen V, Marcellin P, Dhumeaux D, Trinchet JC, Beaugrand M. Noninvasive assessment of liver fibrosis by measurement of stiffness in patients with chronic hepatitis C. Hepatology 2005;41:48–54.
Zwiebel WJ. Sonographic diagnosis of diffuse liver disease. Semin Ultrasound CT MR 1995;16:8–15.